layer in contact with the molten iron of the core would enhance the chemical reactions (*40*), releasing additional Si and O and explaining a possible affinity of CRZs with ULVZs.

References and Notes

1. E. J. Garnero, *Annu. Rev. Earth Planet. Sci.* **28**, 509 (2000).
2. K. E. Bullen, *Mon. Not. R. Astron. Soc. Geophys. Suppl.* **5**, 355 (1949).
3. S. Grand, *J. Geophys. Res.* **99**, 11591 (1994).
4. W.-J. Su, R. L. Woodward, A. M. Dziewonski, *J. Geophys. Res.* **99**, 6945 (1994).
5. T. Lay, D. V. Helmberger, *Geophys. J. R. Astron. Soc.* **75**, 799 (1983).
6. M. H. Weber, *Geophys. J. Int.* **115**, 183 (1993).
7. E. J. Garnero, D. V. Helmberger, *Geophys. Res. Lett.* **23**, 977 (1996).
8. J. Revenaugh, R. Meyer, *Science* **277**, 670 (1997).
9. E. J. Garnero, J. Revenaugh, Q. Williams, T. Lay, L. H. Kellogg, in *The Core-Mantle Boundary Region*, M. Gurnis, M. E. Wysession, E. Knittle, B. Buffett, Eds., vol. 28 of *Geodynamics* (American Geophysical Union, Washington, DC, 1998), pp. 319–334.
10. M. Manga, R. Jeanloz, *Geophys. Res. Lett.* **23**, 3091 (1996).
11. Q. Williams, E. J. Garnero, *Science* **273**, 1528 (1996).
12. E. J. Garnero, R. Jeanloz, *Geophys. Res. Lett.* **27**, 2777 (2000).
13. E. Knittle, R. Jeanloz, *Geophys. Res. Lett.* **15**, 609 (1989).
14. ———, *Science* **251**, 1438 (1991).
15. B. A. Buffett, *Geophys. J. Int.* **125**, 303 (1996).
16. N. L. Montague, L. H. Kellogg, M. Manga, *Geophys. Res. Lett.* **25**, 2345 (1998).
17. Q. Williams, J. Revenaugh, E. Garnero, *Science* **281**, 546 (1998).
18. G. A. Glatzmeier, R. S. Coe, L. Hongre, P. H. Roberts, *Nature* **401**, 885 (1999).
19. B. A. Buffett, E. J. Garnero, R. Jeanloz, *Science* **290**, 1338 (2000).
20. E. J. Garnero, J. E. Vidale, *Geophys. Res. Lett.* **26**, 377 (1999).
21. C. Reasoner, J. Revenaugh, *J. Geophys. Res.* **105**, 28173 (2000).
22. S. E. Persh, J. E. Vidale, P. S. Earle, *Geophys. Res. Lett.* **28**, 387 (2001).
23. Receiver stacks or slant stacks account for the time offset between the individual array recordings due to different incident angles of the wavefront at the array prior to summation of traces. Incoherent noise and coherent phases with deviating incidence angles are suppressed, whereas the phase of interest is amplified.
24. J. C. Castle, R. D. van der Hilst, *Earth Planet. Sci. Lett.* **176**, 311 (2000).
25. M. H. Weber, *Geophys. J. Int.* **92**, 9 (1988).
26. GBM synthetics were compared with computationally intensive reflectivity synthetics [G. Müller, *J. Geophys.* **58**, 153 (1985)] to ensure their accuracy.
27. B. L. N. Kennett, E. R. Engdahl, *Geophys. J. Int.* **105**, 429 (1991).
28. A. M. Dziewonski, D. L. Anderson, *Phys. Earth Planet. Inter.* **25**, 297 (1981).
29. Supplemental material is available at *Science* Online at www.sciencemag.org/cgi/content/full/294/5548/1911/DC1
30. H.-P. Harjes, M. Henger, *Z. Geophys.* **39**, 865 (1973).
31. E. J. Garnero, D. V. Helmberger, *Phys. Earth Planet. Inter.* **91**, 161 (1995).
32. E. J. Garnero, R. Jeanloz, *Science* **289**, 70 (2000).
33. E. Knittle, R. Jeanloz, *J. Geophys. Res.* **96**, 16169 (1991).
34. X. Song, T. J. Ahrens, *Geophys. Res. Lett.* **21**, 153 (1994).
35. J. P. Poirier, V. Malavergne, J. L. LeMouël, in (*9*), pp. 131–137.
36. S. I. Braginsky, *Phys. Earth Planet. Inter.* **111**, 21 (1999).
37. F. Birch, *J. Geophys. Res.* **69**, 4377 (1964).
38. P. S. Earle, P. M. Shearer, *Science* **277**, 667 (1997).
39. P. M. Shearer, M. A. H. Hedlin, P. S. Earle, in (*9*), pp. 37–56.
40. E. Ito, K. Morooka, O. Ujike, T. Kasura, *J. Geophys. Res.* **100**, 5901 (1995).
41. O. Gudmundsson, M. Sambridge, *J. Geophys. Res.* **103**, 7121 (1998).

42. We thank G. Jahnke, C. Wicks, and M. Richards for the WRA data set. G. Glatzmeier and Q. Williams provided helpful comments. Supported by NSF Geophysics and CSEDI.

22 August 2001; accepted 25 October 2001

Detection of Molecular Hydrogen in the Atmosphere of Mars

Vladimir A. Krasnopolsky[1]* and Paul D. Feldman[2]

Four hydrogen (H_2) lines have been detected in a spectrum of Mars observed with the Far Ultraviolet Spectroscopic Explorer. Three of those lines are excited by the solar Lyman β photons. The line intensities correspond to a column H_2 abundance of 1.17 ($\pm$0.13) $\times$ 10^{13} per square centimeter above 140 kilometers on Mars. A photochemical model for the upper atmosphere that simulates the observed H_2 abundance results in an H_2 mixing ratio of 15 $\pm$ 5 parts per million in the lower atmosphere. The H_2 and HD mixing ratios agree with photochemical fractionation of D (deuterium) between H_2O and H_2. Analysis of D fractionation among a few reservoirs of ice, water vapor, and molecular hydrogen on Mars implies that a global ocean more than 30 meters deep was lost since the end of hydrodynamic escape. Only 4% of the initially accreted water remained on the planet at the end of hydrodynamic escape, and initially Mars could have had even more water (as a proportion of mass) than Earth.

Mars' atmosphere has a total pressure of 6 mbar and consists of CO_2 (95.5%), N_2 (2.7%), H_2O [variable amounts, ~150 parts per million (ppm)], products of their photochemistry, and noble gases. Among the photochemical products, CO (0.07%), O, O_2 (0.13%), O_3, H, and NO have been detected (*1, 2*). Photochemical models of the martian atmosphere (*3, 4*) predict a comparatively high (~40 ppm) mixing ratio of H_2.

Despite the low abundance of water vapor in the atmosphere, its dissociation and the subsequent chemistry of the photolysis products play a crucial role in preventing the accumulation of CO and O_2 and therefore supporting the stability of CO_2. Molecular hydrogen forms in Mars' middle atmosphere at 20 to 50 km by the reaction between H and HO_2. H_2 is delivered to the upper atmosphere as a result of atmospheric mixing and diffusion. Decomposition of H_2 to atomic hydrogen by ionospheric processes determines the extent of escape of hydrogen to space and therefore the extent of loss of water from Mars. Although the predicted H_2 mixing ratio is comparatively high, molecular hydrogen was not detected by spacecraft that visited Mars (*5–7*). We observed Mars using the Far Ultraviolet Spectroscopic Explorer (FUSE) to detect and measure H_2 in Mars' upper atmosphere.

FUSE consists of four co-aligned telescopes that cover a range of 904 to 1186 Å (*8*). Each telescope has a diffraction grating and a focal plane assembly with four apertures, and shares two segments at one of two detectors. This results in eight spectra per orbit for each aperture. The spectra consist of 16,384 pixels of ~6.5 mÅ each.

We observed Mars on 12 May 2001, when the heliocentric and geocentric distances of Mars were 1.512 and 0.58 AU (*9*), respectively, with angular diameter = 16.2 arc sec, phase (Sun-Mars-Earth) angle = 24°, solar longitude L_S = 160°, geocentric velocity = −10.4 km s^{-1}, and solar activity index $F_{10.7\ cm}$ = 140. Solar longitude is used to specify seasons on Mars, and L_S = 160° corresponds to 2 September in the terrestrial calendar. The exospheric temperature was T_∞ = 270 K (*10*) for the season and solar activity index during the observation. The observation was made in six FUSE orbits with a total exposure of 5 hours.

The instrument resolving power is $\lambda/\delta\lambda$ = 24,000 for point sources and 5000 for Mars, which was observed with the 30 $\times$ 30 arc sec aperture. The spectral line width is 0.2 Å for this resolving power. Another aperture was used to control the terrestrial airglow foreground, which was very weak at the FUSE altitude of 768 km. We summed 96 observed spectra to obtain composite spectra of Mars and the foreground (*11*). These composite

[1]Department of Physics, Catholic University of America, Washington, DC 20064, USA. [2]Department of Physics and Astronomy, Johns Hopkins University, Baltimore, MD 21218, USA.

*To whom correspondence should be addressed. E-mail: vkrasn@altavista.com

spectra consist of 5688 bins of 50 mÅ each.

Fourteen of the strongest H_2 lines (*12*) that should be in the FUSE spectral range are not blended with other lines (Table 1). All these lines originate from three levels of the upper electronic state $B^1\Sigma_u^+$ of the H_2 Lyman band system. Vibrational and rotational quantum numbers of these levels are $v' = 6$ and $J' = 0$, 11 and 2, and 5 and 2, respectively (*13*). Four of these lines have been detected at a level exceeding 3 statistical uncertainties, and the two strongest lines are shown in Fig. 1.

Emission rate factors $g = \alpha\sigma bI$ (as defined below) are used to transform the observed line intensities to column abundances of emitting species. The lower level for the excitation of all three upper levels is the same: $v'' = 0$, $J'' = 1$. Its population $\alpha = 0.685$ for H_2 at temperature of 270 K was calculated (*14*) taking into account statistical weights associated with the nuclear spin. These weights are equal to 1 and 3 for even and odd rotational quantum numbers, respectively, if an electronic state is even (the H_2 ground state), and are opposite in the case of an odd electronic state (the upper state of the H_2 Lyman band system). Wavelengths and transition probabilities to calculate the integrated absorption cross sections σ (*15*) are taken from (*16*); b is the branching ratio for a line, that is, a ratio of its transition probability to a sum of transition probabilities of all lines emitted from that upper level. I is the solar radiation at the H_2 absorption lines at 1025.93, 972.63, and 1037.15 Å and is equal to 6.6×10^9, 1.76×10^9, and 1.00×10^9 photons $cm^{-2}\ s^{-1}\ Å^{-1}$, respectively, at 1 AU. We took the data for solar minimum from (*17, 18*) and corrected them to the solar mean conditions of our observations($F_{10.7\ cm} = 140$) using (*19*).

Ratios of the line intensities to the calculated emission rate factors are equal to column abundances of H_2 (Table 1). A weighted mean of these values is 2.7 ($\pm$0.3) $\times 10^{13}$ cm^{-2} and corresponds to the detection of H_2 on Mars at the 9σ level.

CO_2 absorbs the solar photons that excite H_2 and the photons emitted by H_2. A convenient approximation for light components on Mars is to assume a black atmosphere below a level where a total two-way optical depth of CO_2 is equal to 1, and to neglect the CO_2 absorption above this level (*20*). This absorption level varies for the H_2 lines from 127 to 148 km, depending on the CO_2 cross sections (*21*), and its mean altitude is 140 $\pm$ 5 km. Intensities in our spectrum of Mars refer to solid Mars with a radius $R = 3390$ km, and the observed H_2 column abundance should be reduced by a factor of $[1 + (140/3390)]^2 = 1.084$.

The obtained H_2 column abundance needs a correction for air mass factor. This factor η is equal to 2 for phase angle $\beta = 0$ and global mean conditions. We have solved the problem for arbitrary β and found

$$\eta = 2 - \frac{2}{\pi}[\beta \sin\beta + (1 - \sin\beta)\tan\beta] \quad (1)$$

Then $\eta = 1.723$ for $\beta = 24°$.

H_2 is a light species with a large scale height (330 km for $T = 270$ K), and the H_2 emission from the dayside limb contributes to the total observed emission. (Scale height is the altitude interval in which density decreases by a factor of $e = 2.72$.) The air mass is much greater on the limb, and this moves the absorption level to ~160 km. Our calculation for the limb takes into account the correction (*22*) for the large scale height of H_2 and results in a term of ~0.73 (*23*) that should be added to get a total correction factor of $(1.084 \times 1.723) + 0.73 = 2.6$. This factor depends weakly on the CO_2 cross sections, and this dependence is taken into account in the calculated vertical column abundances of H_2 (Table 1). The weighted-mean vertical column abundance of H_2 is 1.08 ($\pm$0.12) $\times 10^{13}$ cm^{-2}.

A final correction is for the absorption of the solar photons by H_2 (self-absorption). Photons emitted by H_2 are not absorbed by H_2 molecules because these photons do not involve the ground state $v'' = 0$. Our calculation of self-absorption was made for the (6-0) P1 line at 1025.93 Å that excites three of the four detected H_2 lines. Assuming a mean air mass of 2 for the solar radiation and thermal broadening for this

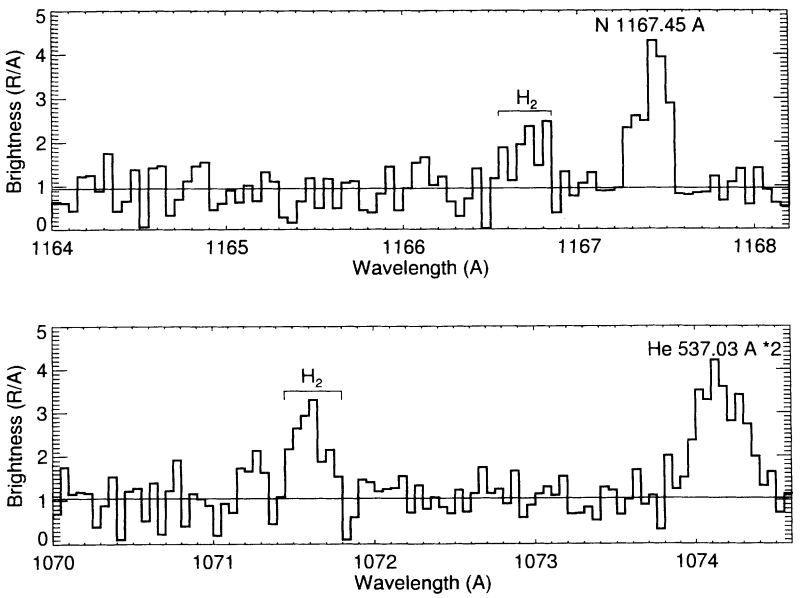

Fig. 1. Fragments of Mars' spectrum near the H_2 lines at 1166.76 and 1071.62 Å. Thin lines show the background.

Table 1. H_2 lines in the FUSE spectrum of Mars. Lines above 3σ detection limit are in italics. Emission rate factors g are calculated for the solar activity index $F_{10.7\ cm} = 140$ and heliocentric distance of 1.512 AU. $4\pi I$ is the brightness in Rayleighs (*6*), which refers to the size of solid Mars and with no correction for both dark crescent and the atmosphere above the dayside limb. $\{H_2\}_{sl}$ is the global-mean slant column abundance of H_2 uncorrected for air mass and self-absorption. $\{H_2\}_0$ is the vertical column abundance of H_2 above 140 km uncorrected for self-absorption. The weighted-mean corrected vertical abundance is equal to 1.17 ($\pm$0.13) $\times 10^{13}$ cm^{-2} from these data. All errors are 1σ.

Line	λ (Å)	g (ph s^{-1})	$4\pi I$ (R)	$\{H_2\}_{sl}$ ($\times 10^{13}$ cm^{-2})	$\{H_2\}_0$ ($\times 10^{13}$ cm^{-2})
(6-1) P1	*1071.62*	*8.54 × 10⁹*	*0.465 ± 0.059*	*5.45 ± 0.69*	*2.07 ± 0.27*
(6-2) P1	*1118.61*	*5.44 × 10⁹*	*0.135 ± 0.033*	*2.48 ± 0.61*	*1.00 ± 0.24*
(6-3) P1	*1166.76*	*1.28 × 10⁸*	0.279 ± 0.058	2.18 ± 0.46	*0.80 ± 0.18*
(11-1) R1	1013.60	7.17 × 10^{10}	0.019 ± 0.072	2.64 ± 10.0	1.04 ± 4.00
(11-1) P3	1019.36	1.22 × 10⁹	0.019 ± 0.041	1.56 ± 3.38	0.62 ± 1.36
(11-2) R1	1055.54	2.84 × 10⁹	0.062 ± 0.033	2.18 ± 1.16	0.84 ± 0.45
(11-2) P3	1061.46	2.63 × 10⁹	0.092 ± 0.059	3.50 ± 2.24	1.39 ± 0.90
(11-3) R1	1098.31	1.31 × 10⁹	0.002 ± 0.077	0.16 ± 5.86	0.06 ± 2.22
(11-3) P3	1104.38	2.33 × 10⁹	0.048 ± 0.077	2.07 ± 3.30	0.78 ± 1.25
(11-4) R1	1141.73	1.63 × 10⁹	0.023 ± 0.054	1.42 ± 3.33	0.55 ± 1.29
(11-4) P3	1147.92	1.12 × 10⁹	0.064 ± 0.045	5.74 ± 4.05	2.16 ± 1.53
(5-0) P3	1043.50	3.54 × 10⁹	−0.035 ± 0.063	−1.0 ± 1.20	−0.37 ± 0.75
(5-1) P3	*1090.45*	*2.66 × 10⁹*	*0.193 ± 0.063*	*7.29 ± 2.38*	*2.77 ± 0.90*
(5-3) R1	1181.29	2.04 × 10⁹	−0.055 ± 0.065	−2.7 ± 3.18	−0.92 ± 1.09

line, its peak cross section is 9×10^{-15} cm^2 from (*15*), and a slant optical depth is $\tau = 2 \times (9 \times 10^{-15}) \times (1.08 \times 10^{13}) = 0.195$ in the line center. The corrected value is $\tau_0 = 0.21$ (*24*), which results in a vertical abundance of H_2 of $1.17 (\pm 0.13) \times 10^{13}$ cm^{-2} above 140 km on Mars.

We modeled self-consistently the density profiles of O, N_2, CO, Ar, He, H_2, H, HD, D, and 18 ions in the range of 80 to 300 km by solving the continuity equations for these species (*25*). The density profiles for H_2, H, HD, and D are shown in Fig. 2. Processes that result in dissociation of H_2 are the reactions with CO_2^+, O^+, CO^+, N_2^+, N^+, Ar^+, and $O(^1D)$, ionization (followed by the ion reactions), and photoelectron dissociation. Similar processes are applied to HD with a correction for the greater mass. We calculated our model for the conditions of our observation, the observation of D (*26, 27*), which is closely relevant to the problem of hydrogen isotope fractionation and loss, and the observation of H from Mariner 6 and Mariner 7 (*20*).

H_2 and HD densities at 80 km were chosen to fit the observed H_2 column abundance above 140 km and the observation of D. They are equal to 4×10^8 and 2.9×10^5 cm^{-3}, respectively. The H_2 density corresponds to its mixing ratio of 15 ± 5 ppm in Mars' lower atmosphere. The given uncertainty mostly reflects the uncertainties of the initial data in our models. The obtained mixing ratio is smaller than the predictions of recent models (*3, 4, 26, 28*) by a factor of 2.7. The obtained HD density results in its mixing ratio of 11 ± 4 parts per billion. The calculated concentration of H = 2.7×10^4 cm^{-3} at 250 km at solar maximum agrees with the Mariner 6 and 7 value of $2.7 (\pm 1) \times 10^4$ cm^{-3} (*20*).

The H_2 and HD densities correspond to

$$\frac{HD/H_2}{HDO/H_2O} = 0.41 \qquad (2)$$

for $HDO/H_2O = 2 \times 5.5$ (*29–31*) times the terrestrial value of D/H = 1.56×10^{-4} (*32*). The currently studied processes of fractionation of D between H_2O and H_2 in the martian lower atmosphere are the depletion in photolysis of HDO relative to that of H_2O (*33*) and the preferential condensation of HDO near and above the hygropause (*34*). A composite effect of these processes was calculated at 0.43 in (*28*), exactly the value we obtain from our observation, the observation of D (*26*), and the model. We do not have any means to fit this value in our model, and this coincidence strongly favors the adequacy of the obtained H_2 and HD abundances. This also solves the controversy between the photochemical and thermodynamical controls of fractionation of D in H_2 relative to H_2O in Mars' atmosphere (*26, 28, 35*) in favor of the photochemical control.

Escape fluxes Φ calculated in our models make it possible to calculate a fractionation factor

$$f = \frac{\Phi_{D+HD}/\Phi_{H+2H_2}}{D/H} \qquad (3)$$

This factor is equal to 0.055, 0.082, and 0.167 at low, medium, and high solar activity, respectively. The sums of the fluxes from three models are used in this relation to determine the mean fractionation factor, which is equal to 0.105.

The analysis of H_2O exchange between a few reservoirs on Mars (*28*) results in

$$a = \frac{1}{f} \ln \frac{1-f}{1-fr} \qquad (4)$$

where a is the ratio of the H_2O loss to the H_2O abundance in the reservoir exchangeable with the atmosphere in the last billion years, and r is the present-to-initial D/H ratio. Most probably, a bulk of the exchangeable reservoir is the ice in the polar caps, which is equal to a global layer ~14 m thick (*28, 36–38*). The polar caps shrink very much or completely disappear at very high obliquity of 40° to 45° (*39, 40*) and accumulate water from the atmosphere at low obliquity. The mean excess of D in H_2O from the martian meteorites (*41, 42*), which had been injected from the upper layers of Mars' regolith, is smaller than that in the atmospheric H_2O by a factor of 2.6. Water in the deep regolith may be depleted in D even more strongly. It is not clear whether the recently found seeps and gullies could involve amounts of water comparable to a global ocean ~100 m deep (a moderate estimate for H_2O in regolith), nor is it clear how effective the isotope exchange with the atmosphere could be for the conditions of fast drainage and freezing out of the erupted water. Therefore, we expect that only a small part of H_2O in the regolith was exchangeable with the atmosphere.

The D/H ratio was probably equal to 1.9 at the end of hydrodynamic escape (*43*). Then $r = 5.5/1.9 = 2.9$, $a = 2.4$, and the loss of water after the end of hydrodynamic escape is 30 m. This value becomes a lower limit if exchange of H_2O in the regolith with the atmosphere was effective during the last billion years.

Hydrogen escape is coupled with escape of oxygen on a long-term scale (*44*). Therefore, our value may be compared with the H_2O loss of 10, 50, and 9 m calculated in (*45–47*), respectively, using a completely different approach: the integration of oxygen escape processes after the end of impact erosion of Mars' atmosphere (*48*).

Hydrodynamic escape of water on Venus could occur when the H_2O/CO_2 volume ratio in the atmosphere exceeded 0.6 (*49*). Evidently, the existence of a liquid H_2O ocean on early Mars is not sufficient to drive hydrodynamic escape. This requires a hot Mars that could be possible during its accretion and a short time after it ended. Hydrodynamic escape of the initially accreted H_2 and H_2 released in the reaction

$$Fe + H_2O \rightarrow FeO + H_2 \qquad (5)$$

could be more effective. The isotope fractionation factor is $f_h = 0.8$ for this escape if $H_2/CO_2 < 0.5$ (*50*). Then a ratio of the initial water abundance, H_2O_i, to that at the end of hydrodynamic escape, H_2O_e, is

$$\frac{H_2O_i}{H_2O_e} = 1.9^{1/(1-f_h)} = 25 \qquad (6)$$

assuming the terrestrial D/H for the initial water (*51*). On the other hand, $H_2O_e = H_2O_{pc} + H_2O_r + H_2O_l > 50$ m (where the subscripts pc, r, and l refer to the polar caps, regolith, and loss, respectively). The terrestrial ocean scaled to the mass and size of Mars is equivalent to a global martian ocean 1 km deep. The above considerations result in $H_2O_i > 1.25$ km, that is, Mars was initially even more rich in water than Earth (*52*). An additional supply of water from comets with D/H ≈ 2 and a possible difference between the initial D/H on Mars and the terrestrial value may affect this scenario and reduce the loss by hydrodynamic escape.

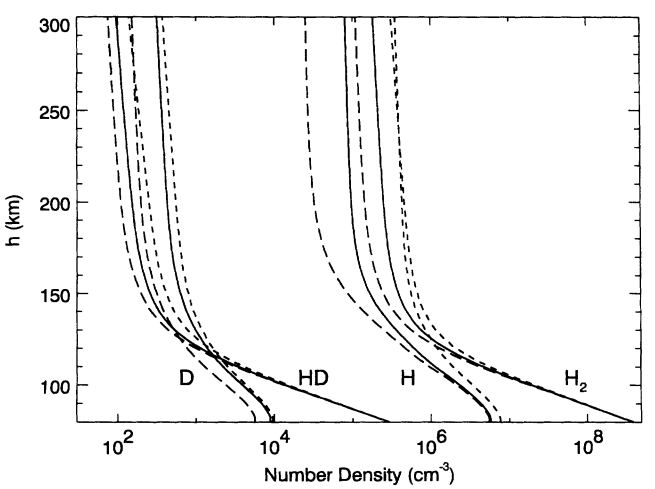

Fig. 2. H_2, H, HD, and D density profiles calculated for the conditions of the observations of D [(*26*), solar minimum, short dashes], H_2 (this work, solar mean, solid lines), and H [(*20*), solar maximum, long dashes].

References and Notes

1. A. O. Nier, M. B. McElroy, *J. Geophys. Res.* **82**, 4341 (1977).
2. T. C. Owen *et al.*, *J. Geophys. Res.* **82**, 4635 (1977).
3. H. Nair, M. Allen, A. D. Anbar, Y. L. Yung, R. T. Clancy, *Icarus* **111**, 124 (1994).
4. V. A. Krasnopolsky, *J. Geophys. Res.* **100**, 3263 (1995).
5. The basic data on the chemical composition of Mars' atmosphere were obtained from the mass spectrometers on the Viking 1 and 2 landing probes that were used to study the upper (*1*) and lower (*2*) atmospheres. However, those mass spectrometers had been designed for masses exceeding 10 and could not detect H_2.
6. An attempt to detect H_2 on Mars by summing the Mariner 9 ultraviolet spectra resulted in an upper limit of 1.5 R to the line at 1607.5 Å that corresponded to the H_2 density of 1.1×10^5 cm^{-3} at 560 km (*53*). One R (Rayleigh) corresponds to a column production of 10^6 photons cm^{-2} s^{-1} $(4\pi$ ster$)^{-1}$.
7. Spectroscopic detection of H_2 presents some difficulties. Despite the low H_2 dissociation energy of 4.48 eV, dissociation to the ground-state H atoms is parity-forbidden, and H_2 absorbs photons only below 1108 Å in the lines of the Lyman and other band systems. The Lyman system converges to the dissociative continuum at 845 Å, which corresponds to the formation of one of the H atoms in the excited state $n = 2$. The solar radiation is weak below 1108 Å, and the fluorescence of H_2 is weak as well. Fortunately, three absorption lines of the H_2 Lyman band system are exceptionally close to the strong solar Lyman β 1025.72 Å, Lyman γ 972.54 Å, and C II 1037.02 Å lines. The differences in the wavelengths are smaller than the widths of the solar lines, and the H_2 emission lines from these three levels are much stronger than other H_2 emission lines. This effect was first observed and explained using the Apollo 17 ultraviolet spectrometer (*54*).
8. B. Blair, B. G. Anderson, Eds., *The FUSE Observer's Guide* (version 3.0, January 2001; http://fuse.pha.jhu.edu/support/guide/guide.html).
9. 1 AU (astronomical unit) is the distance between Earth and the Sun (1.5×10^8 km).
10. S. W. Bougher, S. Engel, R. G. Roble, B. Foster, *J. Geophys. Res.* **105**, 17669 (2000).
11. Eight spectra of Mars and eight foreground spectra were observed at each of six orbits. Wavelengths in each spectrum were adjusted using strong unblended lines of H, O, N, and Ar. Only one of the four telescopes was exactly pointed to Mars, and pointing of the other telescopes was less accurate because of thermal flexture. Exposures, intensities of strong lines, and the known instrument effective areas were used to determine statistical weights for averaging.
12. W. Liu, A. Dalgarno, *Astrophys. J.* **462**, 502 (1996).
13. Some other lines were considered in (*12*) for Jupiter but should be very weak on Mars.
14. The population α was calculated as

$$\alpha(J) = \frac{(2J+1)\, g_s \exp\left[-\dfrac{hcBJ(J+1)}{kT}\right]}{\Sigma\,(2J+1)\, g_s \exp\left[-\dfrac{hcBJ(J+1)}{kT}\right]}$$

where g_s is the nuclear spin statistical weight, $B = 60.853$ cm^{-1} is the H_2 ground-state rotational constant, h and k are the Planck and Boltzmann constants, respectively, and c is the speed of light.

15. The absorption cross sections σ were calculated as

$$\sigma\ (\text{cm}^2\ \text{Å}) = \frac{10^8 A \lambda^4 (2J'+1)}{8\pi c (2J''+1)}$$

Nuclear spins are the same for upper and lower states and cancel out, A is the transition probability, and λ is the wavelength in cm.

16. H. Abgrall, E. Roueff, F. Launay, J.-Y. Roncin, J.-L. Subtil, *Astron. Astrophys. Suppl. Ser.* **101**, 273 (1993).
17. H. P. Warren, J. T. Mariska, K. Wilheim, *Astrophys. J. Suppl. Ser.* **119**, 105 (1998).
18. The H_2 line at 1037.15 Å is near the solar lines at 1036.34, 1037.02, and 1037.61 Å. We fitted the observed maxima and minima of this structure in (*55*) with Gaussians and took into account the instrument resolution of 84 mÅ in (*55*) to obtain the solar intensity at 1037.15 Å.
19. P. G. Richards, J. A. Fennelly, D. G. Torr, *J. Geophys. Res.* **99**, 8981 (1994).
20. D. E. Anderson, C. W. Hord, *J. Geophys. Res.* **76**, 6666 (1971).
21. R. S. Nakata, K. Watanabe, F. M. Matsunaga, *Sci. Light* **14**, 54 (1965).
22. J. W. Chamberlain, D. M. Hunten, *Theory of Planetary Atmospheres* (Academic Press, Orlando, FL, 1987).
23. This term was calculated as

$$0.93\,\frac{(R + 160\ \text{km})(2\pi RH)^{1/2}(1 + 9/8\lambda)}{R^2(1 + 2/\lambda)}$$

where $H = R/\lambda = 331$ km is the H_2 scale height at 160 km for 270 K, $\lambda = \gamma Mm/(RkT) = 10.73$ is the structure parameter, γ is the gravitational constant, M and m are the masses of Mars and H_2, respectively, and 0.93 is a ratio of H_2 column abundances at 160 and 140 km.

24. We deduced the following relation between τ and τ_0:

$$\tau = \frac{2}{\sqrt{\pi}} \int_0^\infty \left\{1 - \exp[-\tau_0 \exp(-x^2)]\right\} dx$$

which is applicable for $\tau_0 < 1$.

25. V. A. Krasnopolsky, in preparation.
26. ———, M. J. Mumma, G. R. Gladstone, *Science* **280**, 1576 (1998).
27. The heliocentric distance of Mars was 1.67 AU, $F_{10.7\ \text{cm}} = 70$, and $T_\infty = 200$ K during the observation (*26*). These values are similar to those from Viking 1 and Viking 2 (*1*, *2*).
28. V. A. Krasnopolsky, *Icarus* **148**, 597 (2000).
29. HDO/H_2O = 2 D/H.
30. T. Owen, J. P. Maillard, C. de Bergh, B. L. Lutz, *Science* **240**, 1767 (1988).
31. V. A. Krasnopolsky, G. L. Bjoraker, M. J. Mumma, D. E. Jennings, *J. Geophys. Res.* **102**, 6525 (1997).
32. R. Hagemann, G. Nief, E. Roth, *Tellus* **22**, 712 (1970).
33. B. M. Cheng *et al.*, *Geophys. Res. Lett.* **26**, 3657 (1999).
34. T. Fouchet, E. Lellouch, *Icarus* **144**, 114 (2000).
35. Y. L. Yung, D. M. Kass, *Science* **280**, 1545 (1998).
36. B. M. Jakosky, *J. Geophys. Res.* **95**, 1475 (1990).
37. D. E. Smith *et al.*, *Science* **284**, 1495 (1999).
38. J. W. Head, *J. Geophys. Res.* **106**, 10075 (2001).
39. J. Touma, J. Wisdom, *Science* **259**, 1294 (1993).
40. B. M. Jakosky, B. G. Henderson, M. T. Mellon, *J. Geophys. Res.* **100**, 1579 (1995).
41. L. L. Watson, I. D. Hutcheon, S. Epstein, E. M. Stolper, *Science* **265**, 86 (1994).
42. L. A. Leshin, S. Epstein, E. M. Stolper, *Geochim. Cosmochim. Acta* **60**, 2635 (1996).
43. L. A. Leshin, *Geophys. Res. Lett.* **27**, 2017 (2000).
44. H. Nair, Y. L. Yung, *Bull. Am. Astron. Soc.* **27**, (1995).
45. We obtained 10 m by integrating the data from table 1 in (*56*) and adding the data for nonthermal escape from (*57*).
46. D. M. Kass, thesis, California Institute of Technology (1999).
47. R. E. Johnson, D. Schnellenberger, M. C. Wong, *J. Geophys. Res.* **105**, 1659 (2000).
48. H. J. Melosh, A. M. Vickery, *Nature* **338**, 487 (1989).
49. J. F. Kasting, J. B. Pollack, *Icarus* **53**, 479 (1983).
50. K. Zahnle, J. F. Kasting, J. B. Pollack, *Icarus* **84**, 502 (1990).
51. This is a standard assumption for calculations of deuterium enrichment in the inner solar system.
52. G. Dreibus, H. Wänke, *Icarus* **71**, 225 (1987).
53. H. W. Moos, *J. Geophys. Res.* **79**, 2887 (1974).
54. P. D. Feldman, W. G. Fastie, *Astrophys. J.* **185**, L101 (1973).
55. W. Curdt *et al.*, *Astron. Astrophys. Suppl. Ser.* **126**, 281 (1997).
56. B. M. Jakosky, R. O. Pepin, R. E. Johnson, J. L. Fox, *Icarus* **111**, 271 (1994).
57. J. G. Luhmann, *J. Geophys. Res.* **102**, 1637 (1997).

58. Supported by the NASA FUSE Guest Investigator Program. V.A.K. thanks A. Dalgarno for consultation.

21 August 2001; accepted 16 October 2001

Mediterranean Sea Surface Radiocarbon Reservoir Age Changes Since the Last Glacial Maximum

Giuseppe Siani,[1]* Martine Paterne,[1]† Elisabeth Michel,[1] Roberto Sulpizio,[3] Alessandro Sbrana,[4] Maurice Arnold,[1,2] Geoffrey Haddad[5]

Sea surface reservoir ages must be known to establish a common chronological framework for marine, continental, and cryospheric paleoproxies, and are crucial for understanding ocean-continent climatic relationships and the paleoventilation of the ocean. Radiocarbon dates of planktonic foraminifera and tephra contemporaneously deposited over Mediterranean marine and terrestrial regions reveal that the reservoir ages were similar to the modern one (~400 years) during most of the past 18,000 carbon-14 years. However, reservoir ages increased by a factor of 2 at the beginning of the last deglaciation. This is attributed to changes of the North Atlantic thermohaline circulation during the massive ice discharge event Heinrich 1.

The reservoir age R_{surf} of surface ocean water (the difference between the ^{14}C age of the sea surface and that of the atmosphere) reflects the balance among ^{14}C production, CO_2 exchange between the atmosphere and ocean, and mixing with ^{14}C-depleted intermediate waters (*1*). The distribution of modern (before 1950) marine reservoir ages correlates closely with the main features of global thermohaline circulation. Surface ages vary from ~400 years in the well-ventilated gyres of the central North and South Pacific and Atlantic Ocean up to ~1200 years